The chondrocyte clock gene *Bmal1* controls cartilage homeostasis and integrity

Michal Dudek,[1] Nicole Gossan,[1] Nan Yang,[1] Hee-Jeong Im,[2] Jayalath P.D. Ruckshanthi,[1] Hikari Yoshitane,[3] Xin Li,[2] Ding Jin,[1] Ping Wang,[1] Maya Boudiffa,[4] Ilaria Bellantuono,[4] Yoshitaka Fukada,[3] Ray P. Boot-Handford,[1,5] and Qing-Jun Meng[1,5]

[1]Faculty of Life Sciences, University of Manchester, Manchester, United Kingdom. [2]Department of Biochemistry, Rush University Medical Center, Jesse Brown VA Medical Center, Chicago, Illinois, USA. [3]Department of Biological Sciences, Graduate School of Science, The University of Tokyo, Tokyo, Japan. [4]The Mellanby Centre, Department of Human Metabolism, The Medical School, Sheffield, United Kingdom. [5]Wellcome Trust Centre for Cell Matrix Research, University of Manchester, Manchester, United Kingdom.

Osteoarthritis (OA) is the most prevalent and debilitating joint disease, and there are currently no effective disease-modifying treatments available. Multiple risk factors for OA, such as aging, result in progressive damage and loss of articular cartilage. Autonomous circadian clocks have been identified in mouse cartilage, and environmental disruption of circadian rhythms in mice predisposes animals to OA-like damage. However, the contribution of the cartilage clock mechanisms to the maintenance of tissue homeostasis is still unclear. Here, we have shown that expression of the core clock transcription factor BMAL1 is disrupted in human OA cartilage and in aged mouse cartilage. Furthermore, targeted *Bmal1* ablation in mouse chondrocytes abolished their circadian rhythm and caused progressive degeneration of articular cartilage. We determined that BMAL1 directs the circadian expression of many genes implicated in cartilage homeostasis, including those involved in catabolic, anabolic, and apoptotic pathways. Loss of BMAL1 reduced the levels of phosphorylated SMAD2/3 (p-SMAD2/3) and NFATC2 and decreased expression of the major matrix-related genes *Sox9*, *Acan*, and *Col2a1*, but increased p-SMAD1/5 levels. Together, these results define a regulatory mechanism that links chondrocyte BMAL1 to the maintenance and repair of cartilage and suggest that circadian rhythm disruption is a risk factor for joint diseases such as OA.

Introduction

Osteoarthritis (OA) is one of the most common joint diseases, causing severe pain and disability, with no effective disease-modifying drugs currently available. One key feature of OA is the progressive degeneration and loss of articular cartilage. Age, mechanical injuries, and chronic inflammation are known risk factors, disrupting the function and viability of chondrocytes and leading to an imbalance between the catabolic and anabolic pathways (1–3). As a weight-bearing tissue, articular cartilage is exposed to the daily loading and unloading cycles associated with the circadian (24-hour) rhythms of rest and activity, and sufferers of OA experience time-of-day dependence in their symptoms (4–6).

The mammalian circadian clock hierarchy includes the central pacemaker in hypothalamic suprachiasmatic nuclei (SCN) and peripheral oscillators in most tissues and cell types. Rhythmic activities of brain and muscle Arnt-like protein 1 (BMAL1) and its dimerization partner CLOCK form the positive arm of the circadian clock (7–10). In the morning, CLOCK and BMAL1 dimerize and activate transcription via E-box elements, including transcription of the mammalian period and cryptochrome genes (the negative arm of the feedback loop). PER and CRY proteins accumulate and multimerize in the cytoplasm during the day, then move back to the nucleus in the evening to inhibit CLOCK and BMAL1 activity, thus inhibiting their own transcription. Previous work identified autonomous cartilage circadian rhythms in mice that became dysregulated with age and upon chronic inflammation (11–14). Moreover, environmental disruption of circadian rhythms in mice (mimicking chronic jet lag) predisposes knee cartilage to OA-like damage (15), further supporting the idea of an involvement of circadian rhythm disruption in OA development.

The core clock transcription factor *Bmal1* is essential for circadian pace making in both the SCN and peripheral tissues (16–21). Critically, cell type–specific KO and rescue experiments have demonstrated a clear tissue-specific function of BMAL1. For example, Marcheva et al. ablated the circadian clock specifically in pancreatic islets of mice. Despite the intact behavioral and SCN rhythms, these mice developed a diabetes mellitus–like disorder, in which insulin release and glucose tolerance was impaired (19). Similarly, tissue-specific disruption of the circadian clock in the liver led to hypoglycemia and increased glucose clearance (20), whereas conditional clock disruption in adipocytes caused obesity (21). Moreover, muscle-specific expression of BMAL1 in the global *Bmal1*-KO mouse model restored wheel-running activity levels and body weight (BW), but failed to rescue the calcific tendon/ligament phenotype (18, 22). It remains unknown whether and how BMAL1 functions in chondrocytes to regulate cartilage tissue homeostasis in mice and humans. The current study combined the analyses of human OA samples, aged mouse tissues, and a chondrocyte-specific *Bmal1*-KO mouse model to demonstrate an essential role for BMAL1 in the normal daily function and integrity of cartilage tissue.

▶ Related Commentary: p. 38

Authorship note: Michal Dudek, Nicole Gossan, and Nan Yang contributed equally to this work.
Conflict of interest: The authors have declared that no conflict of interest exists.
Submitted: May 14, 2015; **Accepted:** October 15, 2015.
Reference information: *J Clin Invest*. 2016;126(1):365–376. doi:10.1172/JCI82755.

Table 1. Size and total number of lesions occurring in different compartments of 6 knees

Lesion size as % of height of uncalcified articular cartilage	Medial tibia	Lateral tibia	Medial femoral condyle	Lateral femoral condyle
2 months				
<10%	13	19	0	12
<11%–30%	8	3	0	3
<31%–50%	6	0	0	0
>50%	0	0	0	0
3 months				
<10%	6	3	1	8
<11%–30%	9	4	0	5
<31%–50%	2	2	0	2
>50%	10	5	0	2
6 months				
<10%	0	2	1	2
<11%–30%	1	3	2	6
<31%–50%	3	2	0	1
>50%	13	7	0	4

Lesions were counted and categorized in 1 knee per animal, and the total number of lesions per category from each age group is presented. n = 6 animals per age group. No such lesions were seen in the knees of WT or 1-month-old cKO mice.

Results

It is currently unknown whether clock factors are altered in human OA. To explore a potential role of BMAL1 in OA, we first used IHC to measure changes in BMAL1 in human articular cartilage in response to OA. The number of BMAL1-positive chondrocytes was progressively reduced in OA cartilage with increasing severity compared with the numbers detected in non-OA human tissue (Figure 1, A and B). Furthermore, Western blotting demonstrated significantly reduced levels of BMAL1 in OA cartilage (Figure 1C), indicating clock defects in OA chondrocytes. Aging is a major risk factor for OA, and we have previously shown that the cartilage circadian rhythm is dampened in aged mice. To test whether the levels of the endogenous clock factors show age-related changes, leading to a compromised circadian rhythm, we compared the number of BMAL1-positive cells in young and aged mouse cartilage tissues. Here, we observed a significant reduction of BMAL1-positive chondrocyte numbers in aged mouse knee cartilage (22–24 months) as compared with young (2–3 months) mouse cartilage (Supplemental Figure 1; supplemental material available online with this article; doi:10.1172/JCI82755DS1). These findings suggest a potential involvement of dysregulated BMAL1 in age-related chondrocyte dysfunction and cartilage diseases.

To investigate the importance of chondrocytic clock without the confounding systemic factors, we generated a chondrocyte-specific *Bmal1*-KO mouse by crossing *Col2a1*^{Cre} mice (23) with *Bmal1*$^{fl/fl}$ mice (24). We confirmed the specific *Bmal1* deletion in *Col2a1 Bmal1*$^{-/-}$ mice using genomic DNA extracted from cartilage, but no deletion was apparent in DNA extracted from lung and liver tissue (Supplemental Figure 2). We performed IHC to confirm the marked reduction of BMAL1-positive chondrocytes in the knee and hip articular cartilage of *Col2a1 Bmal1*$^{-/-}$ mice (Figure 2A and Supplemental Figure 3, A and B). In contrast to the global *Bmal1*-null mice (17), the conditional KO (cKO) mice showed no significant differences in BW (Supplemental Figure 4) or obvious signs of systemic premature aging (data not shown). Therefore, the tissue-specific *Bmal1*-KO model allows appropriate evaluation of the chondrocytic circadian clocks in local physiology and pathology.

These cKO mice were crossed onto a PER2::luc reporter background (25) for the tracking of circadian clock activities. Real-time photon counting and bioluminescence imaging confirmed the loss of circadian rhythms in cartilage tissues (femoral head cartilage and xiphoid cartilage), but not in the SCN, lung, or heart (Figure 2B and Supplemental Videos 1 and 2). This is consistent with the selective nature of *Col2a1*-Cre expression in collagen II–expressing (COL2-expressing) cells. The normal pacemaking properties of the SCN suggested that the locomotion behavioral rhythms of the cKO mice should be intact. Indeed, wheel-running behavioral studies revealed normal rhythmic activity patterns and parameters among WT littermates and cKO mice under both 12-hour light/12-hour dark (LD) and constant darkness (DD) conditions (Figure 2C). We observed no significant differences in the activity levels, period, rhythm strength (measured using the percentage of variance), or duration of activity (Supplemental Figure 5). Therefore, we created a mouse model with specific disruption of the circadian rhythm in cartilage in an otherwise rhythmic body environment, causing an internal desynchrony.

No discernible differences were apparent between WT and cKO mouse knees up to 1 month of age (Supplemental Figure 6). However, from age 2 months onward, progressive degeneration and lesions of the knee articular cartilage became apparent in cKO mice (Figure 3 and Table 1). The lesions were initially characterized by cell damage (with signs of apoptosis) near the tide mark (boundary of calcified and noncalcified cartilage), shown as either empty lacuna or confined loss of tissue, surrounded by cells that have distinct morphology (Figure 3, A and B). In cKO knees from 3- or 6-month-old mice, we found that the lesions were more extensive and severe, with progressive loss of chondrocytes and extracellular matrix (Figure 3A; Supplemental Fig-

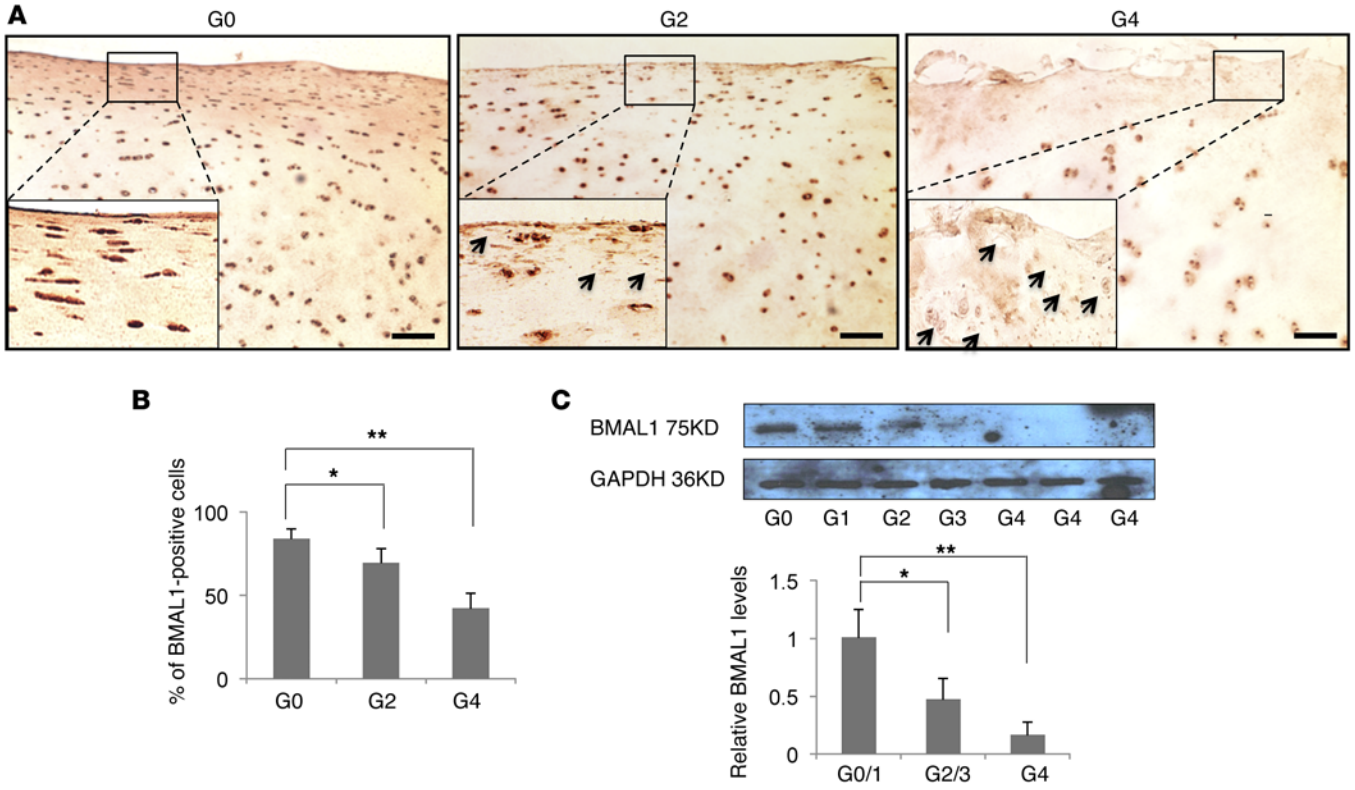

Figure 1. Reduction of BMAL1 expression in articular cartilage from human knees with OA. (**A**) IHC of BMAL1 in full-depth human knee articular cartilage from non-OA (grade 0, G0), grade 2 (G2), or grade 4 (G4) OA samples. Arrows indicate cells with negative or very weak BMAL1 expression. Scale bars: 50 μm. Original magnification, ×3 (insets). (**B**) Quantification of the percentage of cells that stained positive for BMAL1. $^{*}P < 0.05$ and $^{**}P < 0.01$, by nonparametric Mann-Whitney *U* test. $n = 6$ individuals per group. (**C**) Representative Western blot of clinical cartilage samples with various OA scores: grade 0/1, non-OA or mild OA samples ($n = 6$); grade 2/3, moderate OA samples ($n = 6$); and grade 4, OA ($n = 6$). Age range, 45–60 years. For densitometric analysis, the band intensity of BMAL1 was normalized to GAPDH. The average of the G0/1 group was set at 1. $^{*}P < 0.05$ and $^{**}P < 0.01$; 2-way significance was calculated by nonparametric Mann-Whitney *U* test.

ures 7 and 8; and Table 1). X-ray micro-CT analysis and 3D modeling of the tibia subchondral bone demonstrated no significant differences in the subchondral trabecular bone volume fraction (BV/TV), subchondral bone plate thickness and porosity, or any sign of abnormalities at the tibia articular surface in 3-month-old *Bmal1*-cKO mice (Supplemental Figure 9). Despite the profound changes in the articular cartilage, the synovium showed no discernible changes, with no signs of thickening or infiltration of neutrophils (Supplemental Figure 10). In contrast to the global *Bmal1*-KO mouse model (22), x-ray and micro-CT did not detect any signs of ectopic calcification in the ligaments surrounding the knee joint of cKO mice (data not shown). Histological studies also showed no evidence of degeneration in these ligaments (Supplemental Figure 11). The hip articular cartilage remained indistinguishable between WT and cKO mice up to 6 months of age (not shown), despite the significant loss of BMAL1 (Supplemental Figure 3A). This discrepancy between the knee and hip phenotypes could be partially due to the different mechanics of the two joints. Further studies are needed to pinpoint the exact underlying mechanisms. Together, these data demonstrate that the expression of *Bmal1* in chondrocytes is essential for the maintenance of cartilage tissue integrity in the knee.

Cartilage homeostasis is maintained by multiple signaling pathways and key transcription factors (26–29). To reveal genome-wide BMAL1-regulated targets, we performed RNA sequencing (RNA-seq) in WT and cKO cartilage tissues isolated from the femoral heads. This approach revealed a significant number of BMAL1-regulated genes, especially in the groups collected at night (5 am and 9 pm), when the mice were active (Supplemental Table 1). The majority of the BMAL1-regulated genes were time-dependently expressed in WT cartilage tissue and showed constitutive expression in the cKO cartilage (Figure 4A), consistent with the role of BMAL1 as a central regulator of circadian rhythms in gene expression. Gene ontological (GO) profiling revealed more than 100 significant terms, including "role of NFAT in cardiac hypertrophy," "p53 signaling," "WNT/β-catenin signaling," "production of nitric oxide and reactive oxygen species," "IL-1 signaling," "death receptor signaling," and "apoptosis signaling" (Figure 4B). Changes in the rhythmic expression patterns for some classic BMAL1 target clock genes (*Rev-Erba* and *Per2*) were validated by quantitative PCR (qPCR) (Figure 4C).

Ingenuity analysis predicted that the two most significant upstream regulators of the differential genes were TGF-β (inhibited) and TP53 (inhibited). TGF-β signaling plays critical roles in maintaining cartilage metabolic homeostasis and structural integrity (29–33). TGF-β functions via both the ALK5/SMAD-2/3 and the ALK1/SMAD-1/5/8 signaling pathways, which often

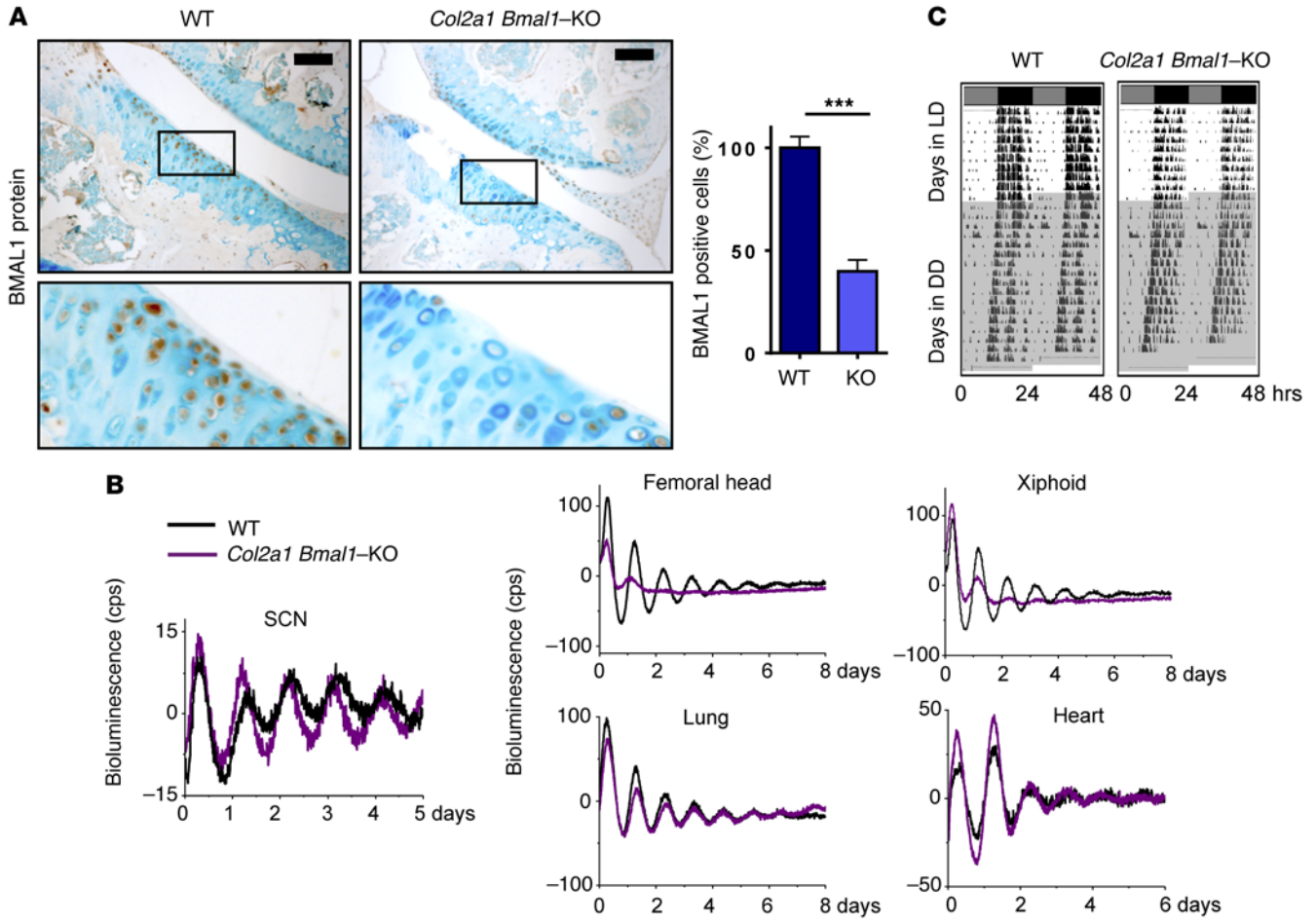

Figure 2. Deletion of chondrocyte *Bmal1* leads to cartilage-specific loss of circadian rhythm. (**A**) Representative BMAL1 IHC (brown) in WT (n = 3 animals/group) and *Col2a1 Bmal1*$^{-/-}$ (n = 4) mouse knee joints. Graph shows quantification of BMAL1-positive cells. Data represent the mean ± SEM. Cells were counted across the entire tibial plateau of anatomically equivalent sections and are expressed as a percentage of WT littermates. ***$P < 0.001$, by 2-tailed Student's t test. Scale bars: 100 μm. (**B**) PER2::luc bioluminescence recordings from SCN and peripheral tissues of WT and *Col2a1 Bmal1*$^{-/-}$ littermates. n = 4 representative traces. cps, counts per second. (**C**) Wheel-running activity records of WT and *Col2a1 Bmal1*$^{-/-}$ littermates under LD or DD conditions. Actograms were double plotted. Upper bar denotes a 12-hour light (gray)/12-hour dark (black) (LD) schedule. Shaded area denotes constant darkness (DD). Black vertical lines denote significant activity in 10-minute bins. Figure shows a representative sample from 1 littermate pair. The experiment was conducted with 6 pairs.

play antagonizing roles (31, 32). Interestingly, in aged and OA cartilage, TGF-β signaling is known to be skewed toward the ALK1/SMAD-1/5/8 pathway, contributing to the catabolic responses of aged and arthritic chondrocytes to TGF-β (29, 31, 32). Indeed, RNA-seq showed that *Alk1 (Acvrl1)* levels were rhythmic in WT mice and constantly upregulated in cKO mice at the night time points (Supplemental Figure 12), while *Alk5 (Tgfbr1)* levels remained unchanged (not shown), suggesting an increase of the *Alk1/Alk5* ratio in cKO cartilage. Using IHC, we demonstrated that the levels of phosphorylated SMAD2 (p-SMAD2) were significantly reduced in cKO mouse knees (Figure 5, A and C), consistent with the reduced mRNA levels for *Ctgf* and *Serpine1*, two classic SMAD2/3 transcriptional targets (Figure 5D). In contrast, we observed increased protein levels of p-SMAD1/5 and mRNA levels of *Id3* (a classic SMAD1/5 target gene) in cKO cartilage (Figure 5, B–D). In primary human articular chondrocytes, knockdown of *BMAL1* shifted TGF-β signaling toward increased p-SMAD1/5 activity, which was associated with an increased *ALK1/ALK5* ratio (Figure 5, E and F). Together, these data identify TGF-β signaling as one of the BMAL1-regulated pathways in mouse and human cartilage, disruption of which might be involved in the degenerative cartilage phenotype of the cKO mouse model.

The downregulation of NFAT signaling, as predicted by Ingenuity analysis, and the reduced *Nfatc2* mRNA levels, as revealed by RNA-seq, in cKO cartilage tissues are intriguing findings. *Nfatc2* was recently identified as a key chondrocyte transcription factor for adult cartilage health (28, 34, 35). Deletion of *Nfatc2* in mice leads to OA-like cartilage degeneration that is associated with increased inflammatory and catabolic pathways and decreased anabolic signaling (e.g., *Sox9*, *Acan*, and *Col2a1*) (35), similar to our RNA-seq results. Interestingly, cartilage damage in *Nfatc2*-KO mice starts at 2 months of age (34, 35), similar to the point at which we started to see cartilage lesions in the cKO mice. The reduced expression of NFATC2 in cKO cartilage tissues was validated by IHC and qPCR (Figure 6, A, C, and D).

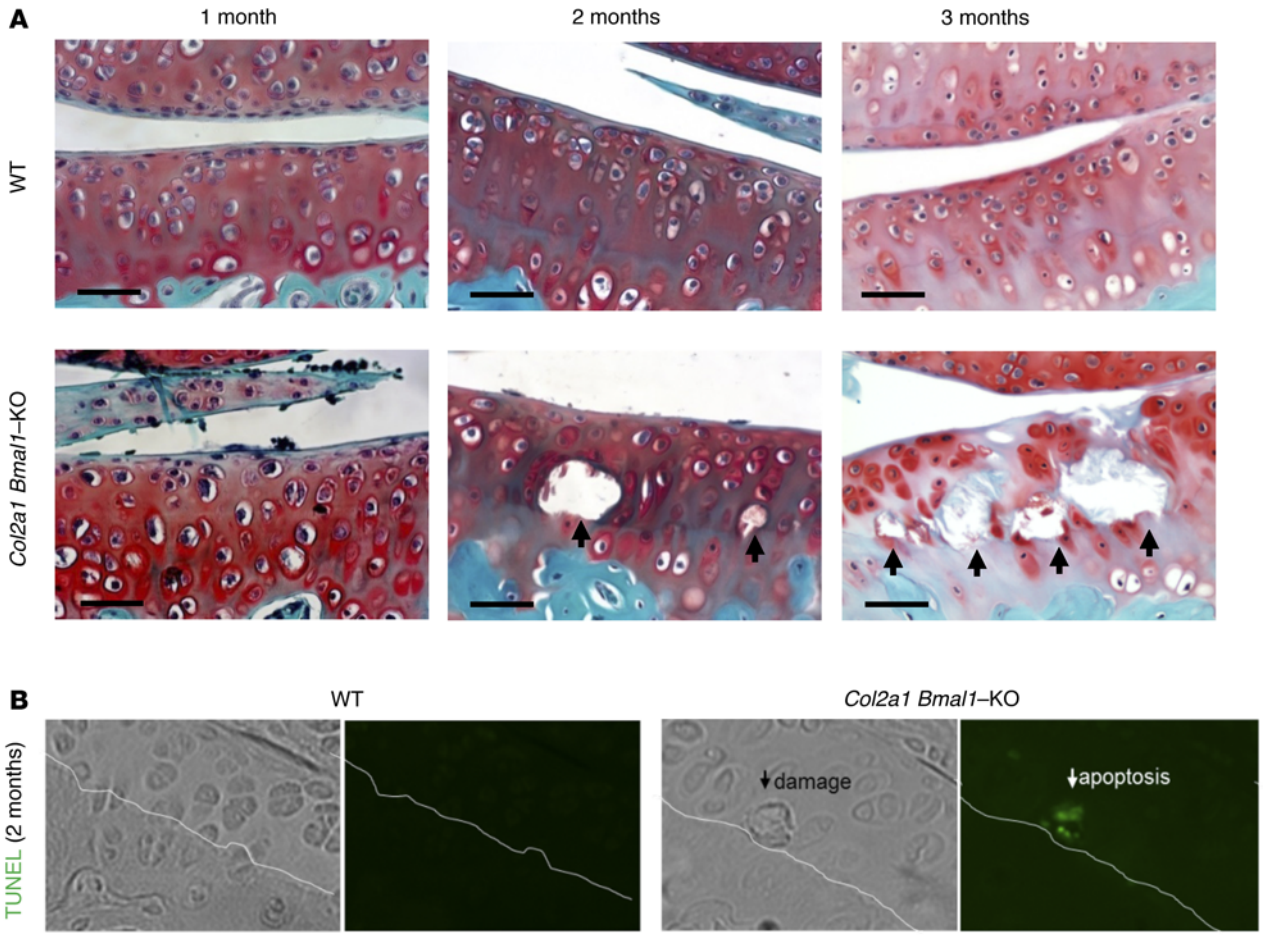

Figure 3. Progressive cartilage degeneration in a *Col2a1 Bmal1*$^{-/-}$ mouse model. (**A**) Representative images of Safranin O, fast green, and hematoxylin staining of knee joint articular cartilage from mice at various ages (n = 9/group). Arrows indicate degeneration and lesions. Scale bars: 50 μm. (**B**) Representative TUNEL staining of cartilage tissues from 2-month-old mice (n = 4). Arrows indicate cartilage damage sites. White lines denote the tide mark. Original magnification, ×20.

Consistent with earlier reports on NFAT-mediated regulation of *Sox9* (35, 36), protein levels of SOX9 were concomitantly reduced in cKO knee cartilage (Figure 6, B and C). Significant reductions of *Sox9*, *Acan*, and *Col2a1* mRNA in cKO cartilage were observed at the 2 night time points (Figure 6D). Our ChIP-seq studies for CLOCK (the binding partner of BMAL1) in mouse liver (37) showed rhythmic binding of CLOCK to a putative E-box–containing region of *Nfatc2* loci (Supplemental Figure 13). ChIP-qPCR confirmed specific binding of CLOCK and BMAL1 to this E-box region in WT mouse cartilage and reduced occupancy of CLOCK or BMAL1 in the *Bmal1*-cKO cartilage (Figure 6E). Functional luciferase assays validated the BMAL1/CLOCK-mediated transactivation of this E-box sequence in cultured cells (Figure 6F). Consistent with the ChIP and luciferase assay results, we validated the rhythmic expression of *Nfatc2* mRNA in temporally collected mouse hip cartilages (Supplemental Figure 14). In primary human articular chondrocytes, we observed that knockdown of *BMAL1* significantly reduced the mRNA levels of *NFATC2* (Figure 6G). Together, our data reveal the endogenous circadian rhythm controlled by the core circadian clock complex (BMAL1 and CLOCK) as a direct temporal control mechanism of NFATC2 in chondrocytes.

Discussion

The presence of a peripheral clock in cartilage tissue has increasingly been recognized. It is well known that there is a daily rhythm to pain and stiffness in arthritic diseases, and the concept of time-dependent pain treatment (chronotherapy) for joint problems was first introduced in the 1980s (38, 39). Our previous work identified autonomous clocks in cartilage tissue and chondrocytes (11, 14). The cartilage circadian rhythms become dampened during aging, upon chronic inflammation, and in mouse models of injury-induced OA (11, 14). However, the current study is the first to our knowledge to demonstrate an essential role of a core clock factor for normal function and structural integrity of articular cartilage. Given the reduced BMAL1 levels we observed in both aged and diseased articular cartilage, it is reasonable to predict that disruption of chondrocyte *Bmal1* expression and/or the circadian rhythm may compromise the daily maintenance and repair of cartilage tissue and become a significant contributing factor in joint diseases such as OA.

It is interesting that our chondrocyte *Bmal1*-cKO mice showed profound and progressive lesions in the articular cartilage that were not found in global *Bmal1*-KO mice (22). The articular cartilage was reportedly normal in global *Bmal1*-KO

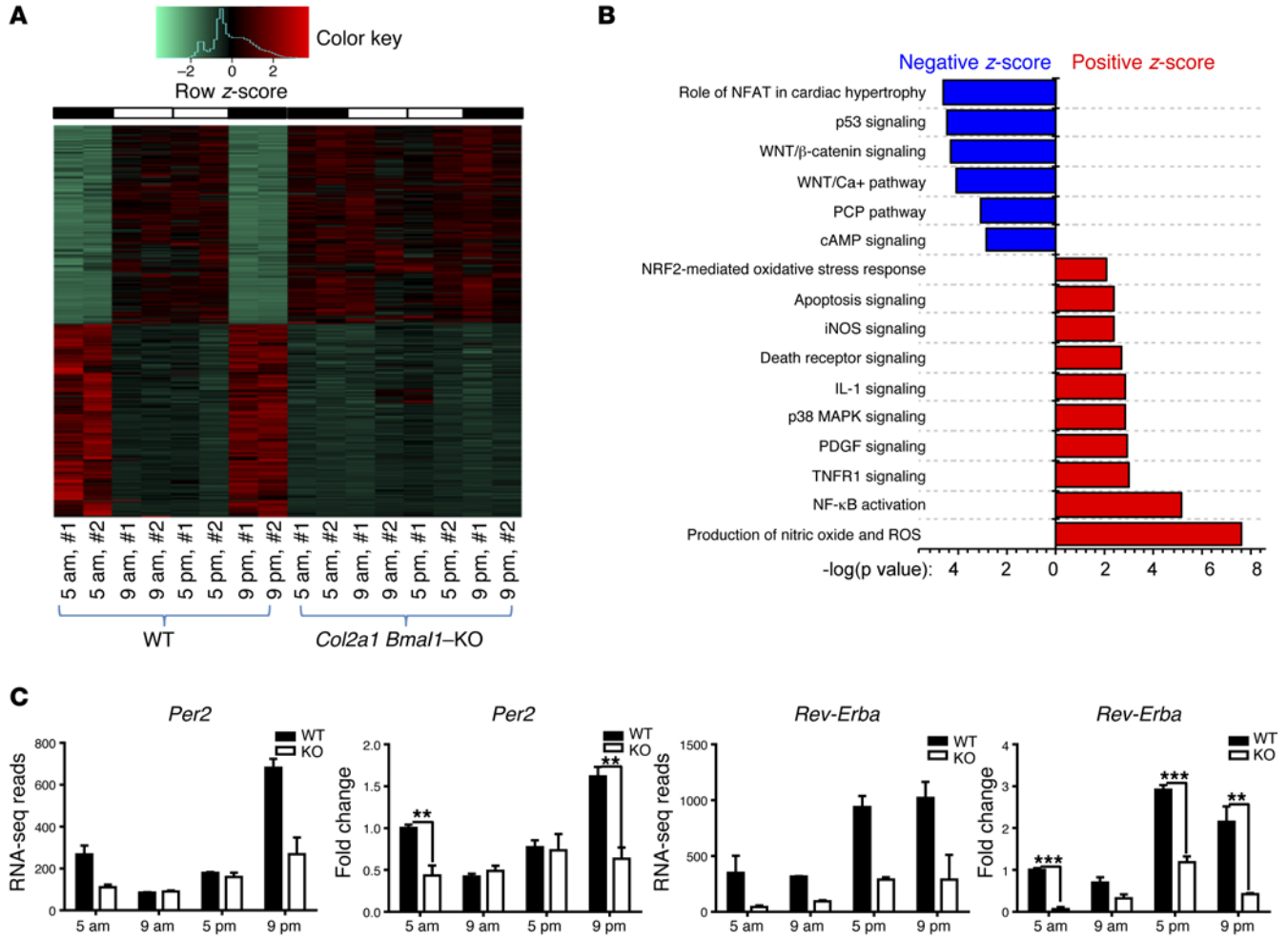

Figure 4. RNA-seq results from cartilage of 8- to 10-week-old WT and *Col2a1 Bmal1*$^{-/-}$ littermates. (**A**) Heatmap depicting expression levels and patterns of the genes identified as significantly different between WT and *Col2a1 Bmal1*$^{-/-}$ cartilages. In total, 5,506 genes were dysregulated in KO cartilages at 1 or more of the 4 time points studied ($\log_2$ fold change >1; adjusted *P* value < 0.05). White bars represent day; black bars represent night. (**B**) GO term analysis of the differentially expressed genes. Selective BMAL1-regulated pathways that are potentially relevant to cartilage homeostasis and OA were plotted against their significant levels (–log *P* value). A positive *z*-score suggests possible upregulation, while a negative *z*-score suggests possible downregulation. (**C**) Several classic BMAL1-regulated clock genes identified in this study were validated by qPCR in mouse cartilage tissue. Data represent the mean ± SEM and were normalized to WT at 5 am and are expressed as relative fold changes (n = 4 animals/time point). All genes tested followed the expression pattern identified by RNA-seq. $^{**}P < 0.01$ and $^{***}P < 0.001$, by 2-tailed Student's *t* test.

mice, despite an arthropathy phenotype that worsened with age (with reduced joint movement, increased stiffness, and ectopic calcification of tendons) (22). One likely explanation for the cartilage damage in the cKO mice is the severe internal desynchrony caused by the specific loss of normal cartilage rhythm in an otherwise rhythmic body environment. It could indicate that chondrocytes in the *Bmal1*-cKO mice are responding inappropriately to rhythmic challenges such as the mechanical loading associated with daily locomotion or other systemic cues. These rhythmic challenges are either abolished or blunted in the whole-body *Bmal1*-KO mouse as a result of systemic loss of rhythms or severe joint immobilization (17, 22). This notion of desynchrony is further supported by the observations that a "chronic jet-lag" schedule in WT mice predisposes them to cartilage degeneration, presumably due to the inability of the local joint clock to adapt to the weekly LD schedule changes (15).

Of note is that the cartilage damage we observed in the *Bmal1*-cKO mice was distinct from that seen in classic OA, which is a whole-joint pathology. The cKO mice demonstrated normal subchondral bone, synovium, and ligaments. This could be partly explained by the conditional cartilage-selective nature of the *Col2a1 Bmal1*–KO mouse, in which the other joint tissues are left intact. Although the expression of *Col2a1*-Cre has been reported in other tissues beyond cartilage (23), the small percentage of *Col2a1*-Cre–positive cells seemed unlikely to have a strong effect on the circadian rhythms of the whole tissue, as observed here in the heart (Supplemental Figure 2). Together, the chondrocyte-selective *Bmal1*-KO mouse model allows proper evaluation of the roles of chondrocyte-expressed BMAL1 and circadian rhythms, eliminating the secondary effects and confounding factors associated with whole-body clock mutant models.

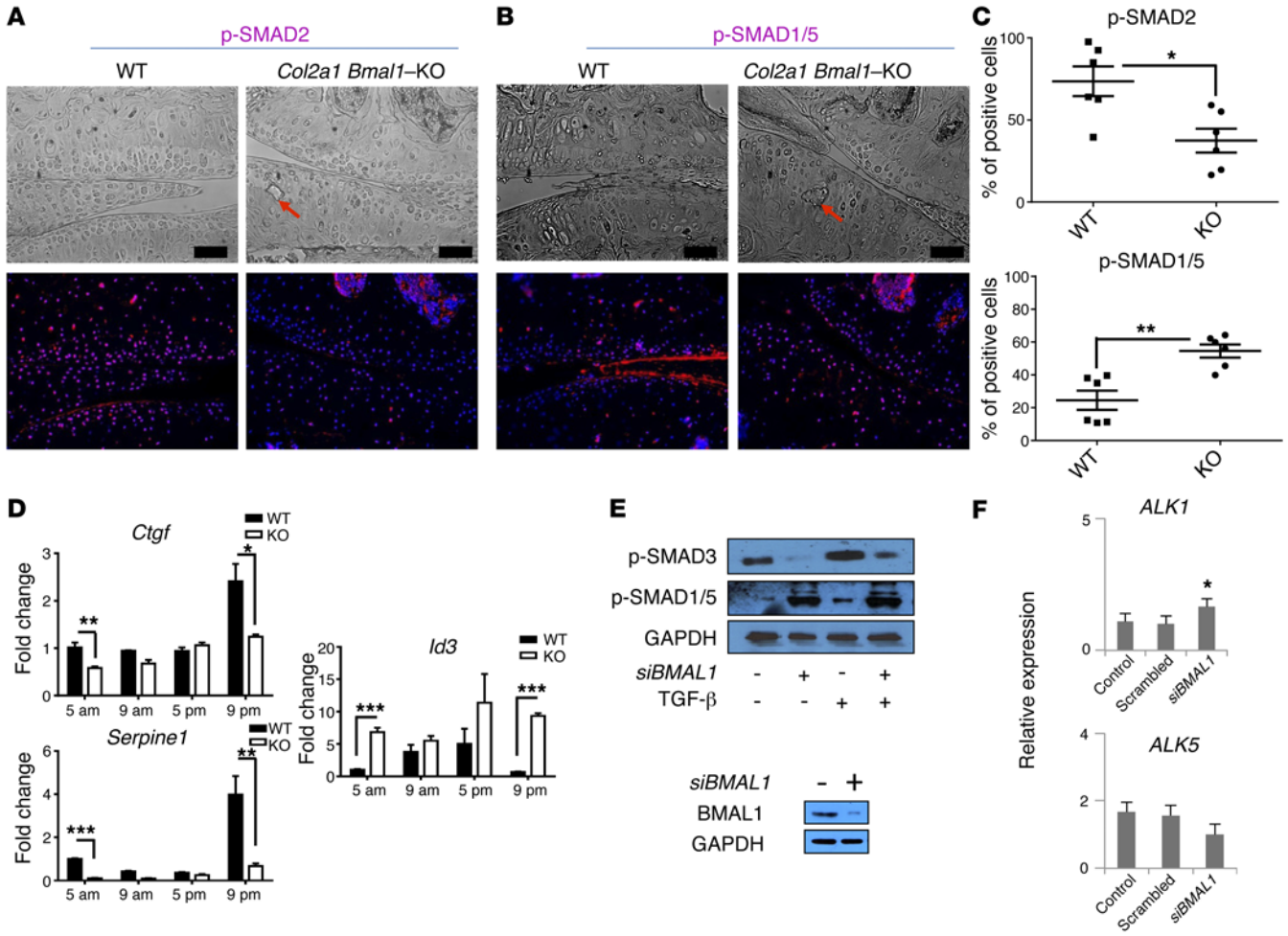

Figure 5. Dysregulated TGF-β signaling in *Col2a1 Bmal1*$^{-/-}$ mouse cartilage. (**A** and **B**) Representative IF images of p-SMAD2 and p-SMAD1/5 in mouse knee joint (n = 6 mice). Red shows positive staining; blue shows DAPI staining. The strong IF signals in the BM were due to nonspecific autofluorescence. Scale bars: 50 μm. (**C**) Quantification of the percentage of IF-positive cells. *P < 0.05 and **P < 0.01, by 2-tailed Student's t test; 2-way significance was calculated by nonparametric Mann-Whitney U test. Data represent the mean ± SEM (n = 6 mice). (**D**) qPCR quantification of mRNA levels of *Ctgf, Serpine1*, and *Id3* in WT and *Col2a1 Bmal1*$^{-/-}$ hip cartilage. Data represent the mean ± SEM and were normalized to WT at 5 am and expressed as relative fold changes (n = 4 animals/time point). *P < 0.05, **P < 0.01, and ***P < 0.001, by 2-tailed Student's t test. (**E**) Western blotting of p-SMAD3 and p-SMAD1/5 in primary human articular chondrocytes after treatment with siRNA targeting *BMAL1,* with and without TGF-β stimulation (100 ng/ml). Scrambled siRNA was used as a control (data not shown). GAPDH was used as a loading control. Representative results are shown for 3 individuals. The knockdown of BMAL1 by siRNA was confirmed by Western blotting. The p-SMAD1/5 blot was derived from parallel samples run on a separate gel. (**F**) *ALK1* and *ALK5* levels were measured by qPCR in primary human articular chondrocytes following knockdown of *BMAL1* (n = 3 individuals). *P < 0.05, by 2-tailed Student's t test.

Our time-series RNA-seq results demonstrated that the majority of the BMAL1-regulated genes were time-dependently expressed in WT cartilage tissue and showed loss of rhythmicity in the cKO cartilage. Although a clock-independent role of BMAL1 cannot be completely ruled out (22, 40), our data strongly support the role of BMAL1 in cartilage maintenance through its function as a central modulator of the circadian rhythm in gene expression. These results, together with the OA-like knee damage seen in mice subjected to environmental disruption of circadian rhythms (15), favor a hypothesis that BMAL1-regulated circadian rhythm is critical for cartilage function. Therefore, the cartilage phenotype observed here is likely due to a combined effect of the circadian dysregulation of multiple pathways. As such, it is perhaps not surprising that the *Bmal1*-cKO cartilage phenotype is not the same as that reported in the *Nfatc2*-KO (28) or postnatal cartilage-selective *Sox9*-KO (41, 42) mouse models. The discrepancies in phenotype between the above-published mouse models and that of our *Bmal1*-cKO mouse remain to be addressed in future studies. Overall, the *Bmal1*-cKO chondrocyte seems to have shifted its phenotype toward a more catabolic state, with reduced TGF-β and NFAT signaling and decreased expression of chondroprotective markers (Supplemental Figure 11). Because of the limited amount and difficulty of dissecting mouse knee articular cartilage, we restricted most of our RNA analysis to mouse hip cartilage, which is much simpler to collect in viable amounts (34). Key pathways (e.g., TGF-β and NFATC2 pathway signaling) that we identified in hip cartilage were validated in knee cartilage using IHC.

The cKO mouse model used in our study showed no overt defects in joint development, BW, or growth rates. Nevertheless, subtle developmental alterations cannot be entirely ruled out,

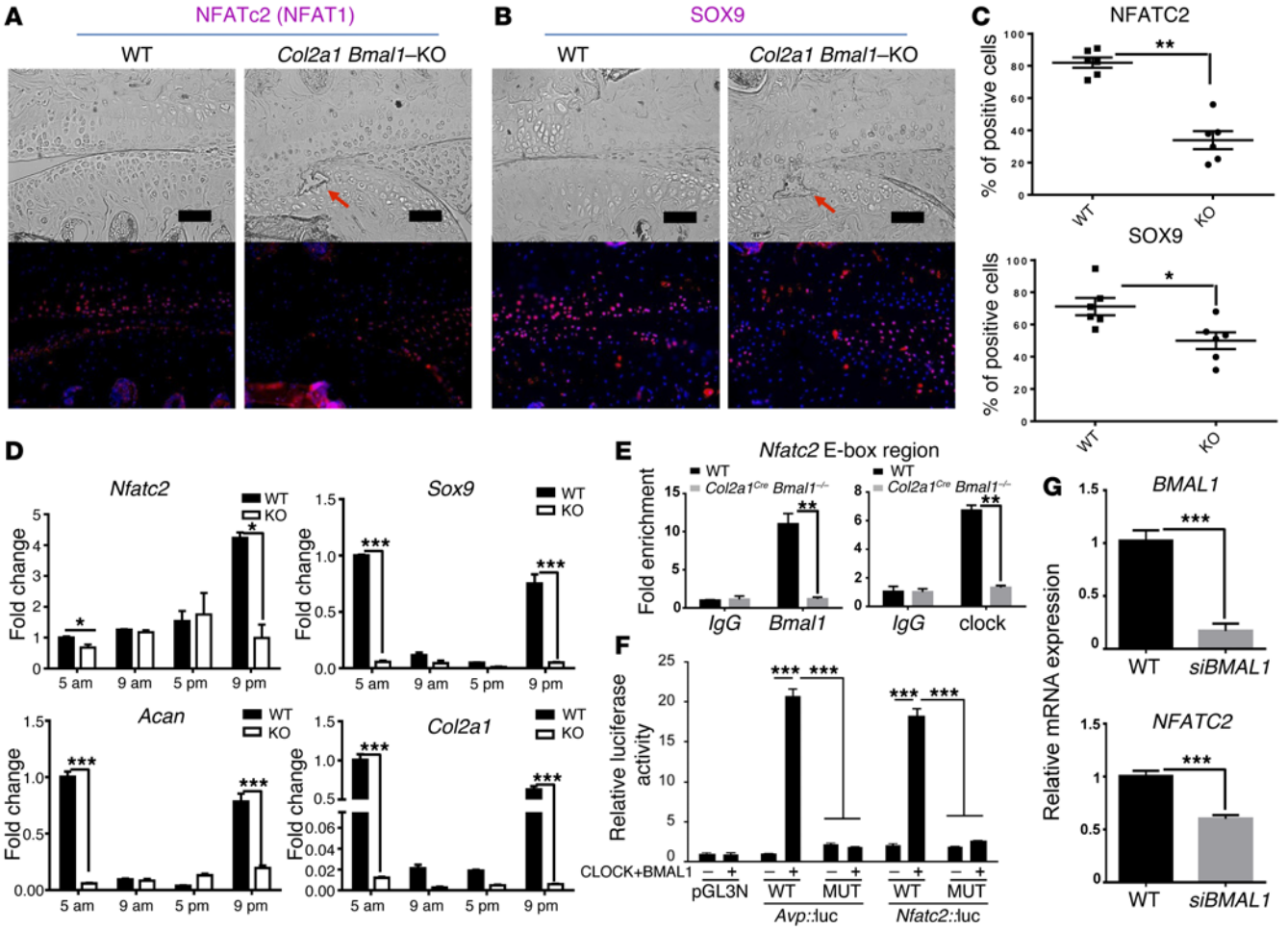

Figure 6. Disrupted circadian control of the NFATC2 pathway in the articular cartilage of *Col2a1 Bmal1*$^{-/-}$ mice. (**A** and **B**) Representative IHC images of NFATC2 and SOX9 in mouse knee joint (n = 6 mice). Scale bars: 50 μm. (**C**) Quantification of the percentage of IF-positive cells. Data represent the mean ± SEM (n = 6 mice). *P < 0.05 and **P < 0.01, by 2-tailed Student's t test; 2-way significance was calculated by nonparametric Mann-Whitney U test. (**D**) qPCR quantification of *Nfatc2*, *Sox9*, *Acan*, and *Col2a1* in WT and KO hip cartilage. Data represent the mean ± SEM (n = 4 mice). *P < 0.05 and ***P < 0.001, by 2-tailed Student's t test. (**E**) Binding of CLOCK or BMAL1 to the E-box–containing region of the *Nfatc2* gene was evaluated in WT and *Bmal1*-cKO femoral head cartilage using CLOCK- or BMAL1-specific ChIP, followed by qPCR. IgG served as a negative control. Data (percentage of input) were normalized to their respective IgG control and are expressed as the mean ± SEM. **P < 0.01, by 2-tailed Student's t test. (**F**) Effects of CLOCK and BMAL1 overexpression on WT or E-box–mutant (MUT) *Nfatc2*::luc activity. Data represent the mean ± SEM and were normalized to pCDNA3.1 control. *Avp*::luc reporter (a classical E-box–regulated promoter) served as a positive control. ***P < 0.001, by 2-tailed Student's t test. (**G**) qPCR quantification of *BMAL1* and *NFATC2* mRNA levels in primary human articular chondrocytes (n = 3 individuals) after treatment with siRNA targeting *BMAL1*. Scrambled siRNA was used as a control. ***P < 0.001, by 2-tailed Student's t test.

and therefore future studies using an inducible KO model in adult mice would lend further support for the role of BMAL1 in the maintenance of tissue homeostasis in postnatal cartilage (43, 44).

In summary, our study provides genetic evidence for and mechanistic insights into a key role of chondrocyte BMAL1 for the normal daily function and integrity of adult articular cartilage. Since cartilage circadian rhythms dampen with aging, the current study suggests that dysregulation of BMAL1 and/or of the circadian clock contributes to disturbances in cartilage homeostasis and may play a role in the development of age-associated diseases such as OA.

Methods

Animals. Mice were maintained at 20°C to 22°C under an LD schedule (light on at 7 am; light off at 7 pm), with ad libitum access to standard rodent chow. *Bmal1*$^{fl/fl}$ mice (24) were crossed onto a PER2::luc background. PER2::luc mice carry the firefly luciferase gene fused in-frame with the 3′ end of the *Per2* gene, creating a fusion protein reporter (25). *Bmal1*$^{fl/fl}$ PER2::luc mice were subsequently crossed with *Col2a1*^{Cre} mice expressing Cre recombinase under the control of the *Col2a1* promoter (23) to generate cartilage-specific *Bmal1*-KO mice. All mice were bred in-house at the University of Manchester.

Genotyping of Col2a1-Bmal1$^{-/-}$ *mice*. DNA was extracted from the ear clips from *Col2a1 Bmal1*$^{-/-}$ mice using a QIAamp DNA Mini Kit (QIAGEN). The PCR reactions were carried out using a *Bmal1* forward primer (5′-CTCCTAACTTGGTTTTTGTCTGT-3′) and a *Bmal1* reverse primer (5′-CTGACCAACTTGCTAACAATTA-3′) with BioMix Red reaction mix (Bioline). The PCR amplification was performed in an Eppendorf Mastercycler pro (VWR International). Cycling conditions were 5 minutes at 95°C with initial denaturation, followed by 38 cycles of 61.6°C, 1 minute for annealing at 72°C,

1 minute for amplification at 72°C, and 5 minutes for the final extension and hold at 4°C. The products were analyzed by 1% agarose gel electrophoresis, stained with SafeView (Applied Biological Materials Inc.), and visualized with Image Analysis Software (Bio-Rad).

Analysis of circadian behavior. Three-month-old male *Col2a1 Bmal1*$^{-/-}$ mice and their WT littermates were individually housed in cages equipped with disposable cardboard running wheels (8 cm in diameter), in light-tight cabinets (Techniplast). The wheels were fitted with a switch to count revolutions and connected to a computer to record activity. A Chronobiology Kit (Stanford Software Systems) was used to record data in 10-minute time bins. Mice were kept under LD cycles for 7 days, then transferred to a DD cycle for an additional 10 days. A Chronobiology Kit was used to analyze wheel-running data with χ^2 periodograms to determine both entrained (LD) and free-running (DD) periods and rhythm strength (45).

Tissue explant cultures and bioluminescence recordings. Organotypic tissue explants for the SCN, lung, heart, and cartilage were prepared as described before (11, 45). Explants were cultured on 0.4-μm cell culture inserts (EMD Millipore), and bioluminescence was recorded in real time using a LumiCycle apparatus (ActiMetrics). Baseline subtraction was performed using a 24-hour moving average.

Live tissue bioluminescence imaging. Cartilage tissue from the femoral heads of WT and *Col2a1 Bmal1*$^{-/-}$ mice (on a PER2::luc background) were imaged using a self-contained Olympus LuminoView LV200 microscope and recorded using a cooled Hamamatsu ImageEM C9100-13 EM-CCD camera (11). Images were taken every hour for 3 days and combined using ImageJ software (NIH).

Human cartilage tissue and chondrocytes, knockdown, and Western blotting. Human cartilage was obtained through the Gift of Hope Organ and Tissue Donor Network, within 24 hours of the death of the donors. Prior to dissection, each specimen was graded for overall degenerative changes on the basis of the modified 5-point scale of Collins (46). Cartilage was dissected and fixed in 4% paraformaldehyde, followed by paraffin embedding for IHC or processed for protein extraction and Western blot analysis to detect BMAL1 (47) or p-SMAD signaling as described previously (15). For the isolation of chondrocytes from non-OA knee joints, cartilage was enzymatically digested with 0.2% pronase for 1 hour, followed by 0.025% collagenase P supplemented with 5% FBS as previously described (15, 48). siRNA transfection studies in isolated primary human articular chondrocytes using nucleofection were described previously (48).

mRNA extraction and qPCR. Hip cartilage was obtained from 8- to 10-week-old mice by dislocating the joint and peeling off the cartilage from the head of the femur using a scalpel blade (35). Careful isolation minimized the possible contamination of the secondary ossification center in these cartilage samples. Cartilage tissues from the left and right hip of the same animal were pooled to obtain sufficient samples. The tissue was immediately snap frozen in liquid nitrogen and then stored at –80°C until mRNA extraction. Tissue was homogenized using a Mikro-Dismembrator S (Satorius Stedim Biotech), with the barrel and ball of the dismembrator precooled in liquid nitrogen. mRNA was extracted using an RNeasy Micro Kit (QIAGEN) according to the manufacturer's protocol. Prepared mRNA was used for RNA-seq and qPCR analysis. For qPCR, RNA concentrations were determined using NanoDrop 2000 (Thermo Scientific), and equal amounts of RNA were converted to cDNA using the High-Capacity cDNA Reverse Transcription Kit (Applied Biosystems, Thermo Fisher Scientific). TaqMan-based qPCR was performed using a StepOnePlus Real-Time PCR System (Applied Biosystems, Thermo Fisher Scientific) with FAST Blue qPCR MasterMix (Eurogentec). TaqMan primers and probes were purchased from Applied Biosystems (Thermo Fisher Scientific). Gene names and probe IDs can be found in Supplemental Table 2.

Histology and IHC. Mouse joints were dissected and fixed in a solution of 4% paraformaldehyde in PBS, followed by decalcification in 20% EDTA, pH 7.4. Decalcified tissues were processed and embedded in paraffin. For the quantification of lesions in the cKO knee histology sections, frontally embedded knee paraffin blocks were sectioned on a microtome to a thickness of 5 μm, with 4 to 5 sections per slide. Each block yielded 40–50 slides. Every fifth slide was stained with Safranin O, and the sections were examined for the presence of lesions in articular cartilage. H&E, Safranin O, and toluidine blue staining were performed according to standard protocols. The lesions were categorized according to the criteria described in Supplemental Figure 8. Lesions occurring in the same place on multiple sections (or on multiple slides in the case of the largest lesions) were counted as 1 lesion. The sum of lesions in each knee compartment, from 6 animals per age group, is presented in Table 1.

IHC and immunofluorescence (IF) were performed using the DAB staining method as described previously (11) or Alexa Fluor 647 fluorescent secondary Abs (Abcam). Briefly, the slides were deparaffinized and rehydrated. Antigen retrieval was performed using 1 mg/ml Trypsin in PBS (Sigma-Aldrich) digestion for 10 minutes. Slides were washed and blocked with blocking solution (3% donkey serum in PBS or TBS [for p-SMAD2 and p-SMAD1/5 Abs] and 0.1% Triton X) for 1 hour at room temperature. The slides were then incubated with a primary Ab diluted in blocking solution overnight at 4°C. Subsequently, slides were washed and incubated with a fluorescent secondary Ab diluted in blocking solution for 1 hour at 4°C. Nuclei were counterstained with Hoechst 33258 (Invitrogen). Methyl green was used as a counter stain for DAB. One of the sections on each slide was used as a no–primary Ab control and to establish the background fluorescence level. Fluorescent images were acquired using Cy5 and DAPI filters on a Zeiss Axio Imager M2 microscope, coupled with a Hamamatsu ORCA-ER digital camera and Micro-Manager software. Images were analyzed with ImageJ software. Sides from 6 WT and 6 cKO animals were used for quantification of the immunofluorescent images. Sections from 2 to 3 slides per animal were imaged, and the number of immune-positive cells per number of DAPI-stained nuclei in noncalcified articular cartilages was counted. The results from individual animals were averaged. Statistical analysis was performed with GraphPad Prism 6.04 (GraphPad Software). The *P* value was calculated using a nonparametric, 2-tailed Mann-Whitney *U* test. All Abs, manufacturers, and catalog numbers are listed in Supplemental Table 2.

Apoptosis assay. The apoptosis assay was carried out on mouse knee sections using a DeadEnd Fluorometric TUNEL System (Promega) according to the manufacturer's protocol for paraffin-embedded tissues. Fluorescent images were acquired using an FITC filter on a Zeiss Axio Imager M2 microscope, coupled with a Hamamatsu ORCA-ER digital camera and Micro-Manager software. Images were analyzed with ImageJ software.

High-resolution micro-CT. Tibiae were dissected, fixed, and scanned using the SkyScan 1172 desktop μCT scanner (Bruker) at a 4.3-μm voxel size. The x-ray source was operated at 50 kV and 200 μA with a 0.5 aluminum filter. Projection images were captured every 0.7° through a 180°

rotation of the bone and were averaged twice. Acquired images were reconstructed with SkyScan NRecon software at a dynamic range of 0.0 to 0.16 and a ring artifact correction of 10. Analysis was performed using SkyScan CT Analyzer software. To measure the subchondral BV/TV, 2 volumes of interest on the medial and lateral sides were chosen for analysis. A standard trabecular bone volume of interest was chosen starting at 0.3 mm above the growth plate and included all the trabeculae in a 1-mm-high section of bone in each subsection. Measurement of subchondral bone plate thickness and porosity selection of the subchondral bone plate volumes of interest were performed on a region of 0.5-mm mediolateral width and 1-mm dorsoventral length of the medial and lateral sides of the load-bearing areas of the tibia plateau. For 3D models, a representative joint from each group was rendered using SkyScan CT Analyzer software. Binary images were obtained using a threshold of 110 over 255; noise was reduced using a Gaussian filter, and the 3D models were generated using the double-time cubes algorithm.

RNA-seq. Total RNA was obtained from the hip cartilage tissues of WT and *Bmal1*-cKO mice, with 2 biological replicates per sample obtained at 5 am (zeitgeber time 22 [ZT22]), 9 am (ZT2), 5 pm (ZT10), and 9 pm (ZT14). The quality and integrity of total RNA samples were assessed using a 2100 Bioanalyzer or a 2200 TapeStation (Agilent Technologies) according to the manufacturer's instructions. RNA-seq libraries were generated using the TruSeq Stranded mRNA assay (Illumina) according to the manufacturer's protocol. Briefly, total RNA (0.1–4 μg) was used as input material from which polyadenylated mRNA was purified using poly-T, oligo-attached magnetic beads. The mRNA was then fragmented using divalent cations under elevated temperature and then reverse transcribed into first-strand cDNA using random primers. Second-strand cDNA was then synthesized with DNA Polymerase I and RNase H (Illumina). Following a single 'A' base addition, adapters were ligated to the cDNA fragments, and the products were then purified and enriched by PCR to create the final cDNA library. Adapter indices were used to multiplex the libraries, which were pooled prior to cluster generation using a cBot instrument (Illumina). The loaded flow cell was then paired-end sequenced (101 plus 101 cycles, plus indices) on an Illumina HiSeq2500 instrument. Demultiplexing of the output data (allowing 1 mismatch) and BCL-to-FastQ conversion were performed with CASAVA 1.8.3. Paired-end reads (101 bp × 101 bp) were generated from each sample. Up to 29 M total reads were obtained for each sample.

Bioinformatics analysis of RNA-seq data. The FastQ files were analyzed with FastQC, and any low-quality reads and contaminated bar codes were trimmed with Trimmomatic (http://www.usadellab.org/cms/index.php?page=trimmomatic). All libraries were aligned to GRCm38.p2 assembly of the mouse genome using Tophat-2.1.0, and only matches with the best score were reported for each read. The mapped reads were counted by genes with HTSeq against Mus_musculus.GRCm38.78.gtf. Time-dependent, differentially expressed (DE) genes were identified by comparing the WT mouse with the *Bmal1*-KO mouse with DESeq2. A "condition" term (WT or KO) and a "time" term were fitted with a linear model. The full model (~condition+time+condition:time) was compared with a reduced model (~condition+time) with DESeq2. The DE genes with an FDR of less than 0.05 and an absolute value of a $\log_2$ fold change of more than 1 were selected for further validation. Raw data were deposited in the ArrayExpress archive of the European Molecular Biology Laboratory–European Bioinformatics Institute (EMBL-EBI) (accession number E-MTAB-3428).

ChIP-qPCR. Freshly harvested hip cartilage tissues were homogenized and cross-linked in 1% (v/v) formaldehyde. The nuclear lysates were sonicated (~500 bp) using Bioruptor NextGen (Diagenode), and 10% of each sheared chromatin sample was saved as input. Following preclearing, hip cartilage chromatin was incubated overnight at 4°C with either rabbit anti-CLOCK (Abcam; catalog ab3715), rabbit anti-BMAL1 (Cell Signaling Technology; catalog 14120), or nonspecific rabbit IgG (Santa Cruz Biotechnology Inc.) for controls. Immunoprecipitated DNA fragments were captured using protein G magnetic Dynabeads (Life Technologies). After a series of washes, proteinase K digestion, and reverse cross-linking, DNA was eluted and cleaned up (QIAGEN). Real-time qPCR was performed using primers specific to the putative E-box region within *Nfatc2* (forward, TCCCCATTTAGCCACACACT; reverse, GCTCTGTTTGGTATGAGGCAG). The experiment was repeated on 3 occasions.

Cloning of the mouse Nfatc2 E-box region. The *Nfatc2* gene has an E-box sequence in its intron 3, to which CLOCK protein rhythmically binds in mouse liver (37). The E-box–containing 200-bp DNA region was cloned from the mouse genome by PCR with gene-specific primers and verified by sequencing. The primers used were *Nfatc2-200bp-Fw3* (GCTAGCAATCGTGACTTCTTTACCAATG) and *Nfatc2-200bp-Rv3* (CTCGAGTGCTCTGTTTGGTATGAGG). The E-box sequence CACGTG was mutated to CAGGTC by PCR with the primers *Nfatc2-Emutaion-Fw* (TCGCTCACACAGCTGAGCCTGAG) and *Nfatc2-Emutaion-Rv* (CCTGAGGAGATGAGTGTGTGGC). The cloned E-box sequences were inserted into an NheI-XhoI site in the pGL3N vector (37), which was modified from a pGL3-Promoter Vector (Promega) for elimination of the basal activity by CLOCK and BMAL1.

Functional luciferase assay. HEK293T cells (American Type Culture Collection [ATCC]) in 24-well plates were transiently transfected with 100 ng Myc-CLOCK/pSG5 and 50 ng BMAL1/pcDNA3.1 in combination with 10 ng firefly luciferase plasmid as a reporter and 1 ng *Renilla* luciferase plasmid (pRL-RSV) as an internal control. The total amount of DNA was adjusted to 311 ng by addition of the empty expression plasmids. The transfected cells were collected 46 hours after transfection and subjected to a dual-luciferase assay by luminometry (Promega) according to the manufacturer's protocol. The values were normalized with the internal control for each cell culture.

Statistics. Data were evaluated using a 2-tailed Student's *t* test or 2-way ANOVA. For the human studies, 2-way significance was calculated by a nonparametric Mann-Whitney *U* test. A *P* value of less than 0.05 was considered statistically significant. Results are presented as the mean ± SEM from at least 3 independent experiments.

Study approval. All animal studies were performed in accordance with the 1986 UK Home Office Animal Procedures Act. Approval was provided by the Animal Welfare Ethical Review Board (AWERB) of the University of Manchester (approval no. 50/2506). Human cartilage was obtained through the Gift of Hope Organ and Tissue Donor Network within 24 hours of the death of the donors, with informed consent obtained from the families and approval provided by the Rush University Medical Center Research and Clinical Trials Administration Committee (Institutional Review Board no. 1, Institutional Federalwide Assurance no. 00000482). Human tissues were handled in strict accordance with the guidelines of the Human Investigation Committee of Rush University Medical Center.

Author contributions

QJM and RPBH designed the experiments. MD, NG, NY, HJI, JPDR, HY, XL, DJ, MB, IB, and QJM conducted the experiments. MD, NG, NY, HJI, JPDR, HY, XL, DJ, PW, MB, and QJM acquired the data. MD, NG, NY, HJI, JPDR, HY, XL, DJ, PW, MB, IB, YF, RPBH, and QJM analyzed the data. QJM and RPBH wrote the manuscript.

Acknowledgments

This work was funded by a Medical Research Council (MRC) UK Career Development Award (G0900414, to Q.J. Meng); an Arthritis Research UK Senior Research Fellowship Award (20875, to Q.J. Meng); an MRC project grant (MR/K019392/1, to Q.J. Meng and R.P. Boot-Handford); a Wellcome Trust (UK) Core funding grant (088785/Z/09/Z) to the University of Manchester Wellcome Trust Centre for Cell Matrix Research; an NIH/NIAMS R01 grant (AR062136, to H.J. Im); an NIH/NIAMS R21 grant (AR067935, to H.J. Im); a Veterans Affairs (VA) BLD&R Merit Review Award (USA) (I01BX002647, to H.J. Im); an Arthritis Foundation (Delivery on Discovery Program) grant (368521, to H.J. Im); and Grants-in-Aid for Scientific Research from MEXT of Japan (to H. Yoshitane and Y. Fukada). The authors thank the Genomic Technologies, Histology, and Bioimaging Core Facilities of the Faculty of Life Sciences of the University of Manchester for providing technical support and advice. We also thank Joseph Takahashi of the University of Texas Southwestern Medical Center for the PER2::luc mice, and Professors Tim Hardingham, Tony Day, Cay Kielty, and Richard Grencis (University of Manchester) for their comments on the manuscript. We thank the Gift of Hope Organ Tissue Donor Network as well as S. Chubinskaya and A. Margulis for making human tissue samples available. We also extend our appreciation to the families of the tissue donors who made these studies possible.

Address correspondence to: Qing-Jun Meng, Faculty of Life Sciences, University of Manchester, Oxford Road, Manchester, M13 9PT, UK. Phone: 44.161.3068912; E-mail: qing-jun.meng@manchester.ac.uk. Or to: Ray Boot-Handford, Wellcome Trust Centre for Cell Matrix Research, University of Manchester, Oxford Road, Manchester, M13 9PT, UK. Phone: 44.161.2755097; E-mail: ray.boot-handford@manchester.ac.uk.

1. Aigner T, Kurz B, Fukui N, Sandell L. Roles of chondrocytes in the pathogenesis of osteoarthritis. *Curr Opin Rheumatol*. 2002;14(5):578–584.
2. Anderson S, Loeser R. Why is osteoarthritis an age-related disease? *Best Pract Res Clin Rheumatol*. 2010;24(1):15–26.
3. Goldring MB, Otero M. Inflammation in osteoarthritis. *Curr Opin Rheumatol*. 2011;23(5):471–478.
4. Bellamy N, Sothern RB, Campbell J, Buchanan WW. Circadian rhythm in pain, stiffness and manual dexterity in rheumatoid arthritis: relation between discomfort and disability. *Ann Rheum Dis*. 1991;50(4):243–248.
5. Bellamy N, Sothern R, Campbell J, Buchanan WW. Rhythmic variations in pain, stiffness and manual dexterity in hand osteoarthritis. *Ann Rheum Dis*. 2002;61(12):1075–1080.
6. Smolensky MH, et al. Diurnal and twenty-four hour patterning of human diseases: acute and chronic common and uncommon medical conditions. *Sleep Med Rev*. 2015;21(14):12–22.
7. Reppert SM, Weaver DR. Coordination of circadian timing in mammals. *Nature*. 2002;418(4901):935–941.
8. Hastings MH, Reddy AB, Maywood ES. A clockwork web: circadian timing in brain and periphery, in health and disease. *Nat Rev Neurosci*. 2003;4(8):649–661.
9. Roenneberg T Merrow M. Circadian clocks-the fall and rise of physiology. *Nat Rev Mol Cell Biol*. 2005;6(12):965–971.
10. Takahashi JS, Hong HK, Ko CH, McDearmon EL. The genetics of mammalian circadian order and disorder: implications for physiology and disease. *Nat Rev Genetics*. 2008;9(10):764–775.
11. Gossan N, et al. The circadian clock in chondrocytes controls key aspects of cartilage homeostasis. *Arthritis Rheum*. 2013;65(9):2334–2345.
12. Honda KK, et al. Different circadian expression of major matrix-related genes in various types of cartilage: modulation by light–dark conditions. *J Biol Chem*. 2013;154(4):373–381.
13. Takarada T, et al. Clock genes influence gene expression in growth plate and endochondral ossification in mice. *J Biol Chem*. 2012;287(43):36081–36095.
14. Guo B, et al. Catabolic cytokines disrupt the circadian clock and the expression of clock-controlled genes in cartilage via an NFκB-dependent pathway. *Osteoarthritis Cartilage*. 2015;23(11):1981–1988.
15. Kc R, et al. Environmental disruption of circadian rhythm predisposes mice to osteoarthritis-like changes in knee joint. *J Cell Physiol*. 2015;230(9):2174–2183.
16. Bunger M, et al. Mop3 is an essential component of the master circadian pacemaker in mammals. *Cell*. 2000;103(7):1009–1017.
17. Kondratov R, Kondratova A, Gorbacheva V, Vykovanets O, Antoch M. Early aging and age-related pathologies in mice deficient in BMAL1, the core component of the circadian clock. *Genes Dev*. 2006;20(14):1868–1873.
18. McDearmon EL, et al. Dissecting the functions of the mammalian clock protein BMAL1 by tissue-specific rescue in mice. *Science*. 2006;314(5803):1304–1308.
19. Marcheva B, et al. Disruption of the clock components CLOCK and BMAL1 leads to hyperinsulinaemia diabetes. *Nature*. 2010;466(7306):627–631.
20. Lamia KA, Storch KF, Weitz CJ. Physiological significance of a peripheral tissue circadian clock. *Proc Natl Acad Sci U S A*. 2008;105(39):15172–15177.
21. Paschos G, et al. Obesity in mice with adipocyte-specific deletion of clock component Arntl. *Nat Med*. 2012;18(12):1768–1777.
22. Bunger MK, et al. Progressive arthropathy in mice with a targeted disruption of the Mop3/Bmal-1 locus. *Genesis*. 2005;41(3):122–132.
23. Sakai K, et al. Stage-and tissue-specific expression of a Col2a1-Cre fusion gene in transgenic mice. *Matrix Biol*. 2001;19(8):761–767.
24. Storch KF, et al. Intrinsic circadian clock of the mammalian retina: importance for retinal processing of visual information. *Cell*. 2007;130(4):730–741.
25. Yoo SH, et al. PERIOD2::LUCIFERASE real-time reporting of circadian dynamics reveals persistent circadian oscillations in mouse peripheral tissues. *Proc Natl Acad Sci U S A*. 2004;101(15):5539–5546.
26. Houard X, Goldring MB, Berenbaum F. Homeostatic mechanisms in articular cartilage and role of inflammation in osteoarthritis. *Curr Rheumatol Rep*. 2013;15(11):375–384.
27. Loeser RF. Aging and osteoarthritis: the role of chondrocyte senescence and aging changes in the cartilage matrix. *Osteoarthritis Cartilage*. 2009;17(8):971–979.
28. Greenblatt MB, et al. NFATc1 and NFATc2 repress spontaneous osteoarthritis. *Proc Natl Acad Sci U S A*. 2013;110(49):19914–19919.
29. Baugé C, Girard N, Lhuissier E, Bazille C, Boumediene K. Regulation and role of TGFβ signaling pathway in aging and osteoarthritis joints. *Aging Dis*. 2013;5(6):394–405.
30. Shen J, et al. Deletion of the Type II TGF-β receptor gene in articular chondrocytes leads to a progressive OA-like phenotype in mice. *Arthritis Rheum*. 2013;65(12):3107–3119.
31. van der Kraan PM, Blaney Davidson EN, Blom A, van den Berg WB. TGF-β signaling in chondrocyte terminal differentiation and osteoarthritis: modulation and integration of signaling pathways through receptor-Smads. *Osteoarthritis Cartilage*. 2009;17(12):1539–1545.
32. Finnson KW, Parker WL, ten Dijke P, Thorikay M, Philip A. ALK1 opposes ALK5/Smad3 signaling expression of extracellular matrix components in human chondrocytes. *J Bone Miner Res*. 2008;23(6):896–906.
33. van Beuningen HM, Glansbeek HL, van der Kraan PM, van den Berg WB. Osteoarthritis-like changes in the murine knee joint resulting from intra-articular transforming growth factor beta injections. *Osteoarthritis Cartilage*. 2000;8(1):25–33.

34. Rodova M, et al. Nfat1 regulates adult articular chondrocyte function through its age-dependent expression mediated by epigenetic histone methylation. *J Bone Miner Res*. 2011;26(8):1974–1986.
35. Wang J, et al. Transcription factor Nfat1 deficiency causes osteoarthritis through dysfunction of adult articular chondrocytes. *J Pathol*. 2009;219(2):163–172.
36. Lin SS, Tzeng BH, Lee KR, Smith RJ, Campbell KP, Chen CC. Cav3.2 T-type calcium channel is required for the NFAT-dependent Sox9 expression in tracheal cartilage. *Proc Natl Acad Sci U S A*. 2014;111(19):E1990–1998.
37. Yoshitane H, et al. CLOCK-controlled polyphonic regulation of circadian rhythms through canonical and noncanonical E-boxes. *Mol Cell Biol*. 2014;34(10):1776–1787.
38. Bellamy N, Sothern R, Campbell J, Buchanan W. Rhythmic variations in pain, stiffness and manual dexterity in hand osteoarthritis. *Ann Rheum Dis*. 2002;61(12):1075–1080.
39. Levi F, LeLoarn C, Reinberg A. Timing optimises sustained-release indomethacin treatment of osteoarthritis. *Clin Pharmacol Ther*. 1985;37(1):77–84.
40. Saito T, et al. Transcriptional regulation of endochondral ossification by HIF-2α during skeletal growth osteoarthritis development. *Nat Med*. 2010;16(6):678–686.
41. Henry SP, Liang S, Akdemir KC, de Crombrugghe B. The postnatal role of Sox9 in cartilage. *J Bone Miner Res*. 2012;27(12):2511–2525.
42. Kist R, Schrewe H, Balling R, Scherer G. Conditional inactivation of Sox9: a mouse model for campomelic dysplasia. *Genesis*. 2002;32(2):121–123.
43. Ono N, Ono W, Nagasawa T, Kronenberg HM. A subset of chondrogenic cells provides early mesenchymal progenitors in growing bones. *Nat Cell Biol*. 2014;16(12):1157–1167.
44. Nagao M, Cheong CW, Olsen B. Col2-Cre and tamoxifen-inducible Col2-CreER target different cell populations in the knee joint [published online ahead of print August 6, 2015]. *Osteoarthritis Cartilage*. doi:10.1016/j.joca.2015.07.025.
45. Meng QJ, et al. Setting clock speed in mammals: the CK1ετ mutation in mice accelerates circadian pacemakers by selectively destabilizing PERIOD proteins. *Neuron*. 2008;58(1):78–88.
46. Muehleman C, Bareither D, Huch K, Cole AA, Kuettner KE. Prevalence of degenerative morphological changes in the joints of the lower extremity. *Osteoarthritis Cartilage*. 1997;5(1):23–37.
47. Sládek M, et al. Insight into the circadian clock within rat colonic epithelial cells. *Gastroenterology*. 2007;133(4):1240–1249.
48. Muddasani P, et al. Basic Fibroblast Growth Factor-mediated activation of the MAPK and NFκB pathways that converge on Elk-1 to control production of matrix metalloproteinase-13 by human adult articular chondrocytes. *J Biol Chem*. 2007;282(43):31409–31421.